

Characterizing extracellular diffusion properties using diffusion-weighted MRS of sucrose injected in mouse brain

Mélissa Vincent, Mylène Gaudin, Covadonga Lucas-torres, Alan Wong, Carole Escartin, Julien Valette

▶ **To cite this version:**

Mélissa Vincent, Mylène Gaudin, Covadonga Lucas-torres, Alan Wong, Carole Escartin, et al.. Characterizing extracellular diffusion properties using diffusion-weighted MRS of sucrose injected in mouse brain. NMR in Biomedicine, 2021, 34 (4), pp.e4478. 10.1002/nbm.4478 . cea-03126700

HAL Id: cea-03126700
https://cea.hal.science/cea-03126700

Submitted on 1 Feb 2021

HAL is a multi-disciplinary open access archive for the deposit and dissemination of scientific research documents, whether they are published or not. The documents may come from teaching and research institutions in France or abroad, or from public or private research centers.

L'archive ouverte pluridisciplinaire **HAL**, est destinée au dépôt et à la diffusion de documents scientifiques de niveau recherche, publiés ou non, émanant des établissements d'enseignement et de recherche français ou étrangers, des laboratoires publics ou privés.



Distributed under a Creative Commons Attribution 4.0 International License

Check for updates

Received: 23 July 2020 | Accepted: 4 January 2021

DOI: 10.1002/nbm.4478

RESEARCH ARTICLE

NMR IN BIOMEDICINE WILEY

Characterizing extracellular diffusion properties using diffusion-weighted MRS of sucrose injected in mouse brain

Mélissa Vincent[1,2] | Mylène Gaudin[1,2] | Covadonga Lucas-Torres[3] | Alan Wong[3] | Carole Escartin[1,2] | Julien Valette[1,2]

[1]Commissariat à l'Energie Atomique et aux Energies Alternatives (CEA), Molecular Imaging Research Center (MIRCen), Fontenay-aux-Roses, France

[2]Commissariat à l'Energie Atomique et aux Energies Alternatives (CEA), Centre National de la Recherche Scientifique (CNRS), Université Paris-Saclay, UMR 9199 (Neurodegenerative Diseases Laboratory), Fontenay-aux-Roses, France

[3]Centre National de la Recherche Scientifique (CNRS), Commissariat à l'Energie Atomique et aux Energies Alternatives (CEA), Université Paris-Saclay, Nanosciences et Innovation pour les Matériaux, la Biomédecine et l'Energie (NIMBE), Gif-sur-Yvette, France

Correspondence
Julien Valette, Commissariat à l'Energie Atomique et aux Energies Alternatives (CEA), MIRCen, 18 Route du Panorama, 92260, Fontenay-aux-Roses, France.
Email: julien.valette@cea.fr

Brain water and some critically important energy metabolites, such as lactate or glucose, are present in both intracellular and extracellular spaces (ICS/ECS) at significant levels. This ubiquitous nature makes diffusion MRI/MRS data sometimes difficult to interpret and model. While it is possible to glean information on the diffusion properties in ICS by measuring the diffusion of purely intracellular endogenous metabolites (such as NAA), the absence of endogenous markers specific to ECS hampers similar analyses in this compartment. In past experiments, exogenous probes have therefore been injected into the brain to assess their apparent diffusion coefficient (ADC) and thus estimate tortuosity in ECS. Here, we use a similar approach in mice by injecting sucrose, a well-known ECS marker, in either the lateral ventricles or directly in the prefrontal cortex. For the first time, we propose a thorough characterization of ECS diffusion properties encompassing (1) short-range restriction by looking at signal attenuation at high b values, (2) tortuosity and long-range restriction by measuring ADC time-dependence at long diffusion times and (3) microscopic anisotropy by performing double diffusion encoding (DDE) measurements. Overall, sucrose diffusion behavior is strikingly different from that of intracellular metabolites. Acquisitions at high b values not only reveal faster sucrose diffusion but also some sensitivity to restriction, suggesting that the diffusion in ECS is not fully Gaussian at high b. The time evolution of the ADC at long diffusion times shows that the tortuosity regime is not reached yet in the case of sucrose, while DDE experiments suggest that it is not trapped in elongated structures. No major difference in sucrose diffusion properties is reported between the two investigated routes of injection and brain

Abbreviations used: ADC, apparent diffusion coefficient; CRLB, Cramér-Rao lower bound; CSF, cerebrospinal fluid; DDE, double diffusion encoding; D_{free}, free diffusion coefficient; DKI, diffusion kurtosis imaging; DTI, diffusion tensor imaging; DW-MRI, diffusion-weighted MRI; DW-MRS, diffusion-weighted NMR spectroscopy; ECM, extracellular matrix; ECS, extracellular space; HBSS, Hank's balanced salt solution; HR-MAS, high-resolution magic angle spinning; ICS, intracellular space; LASER, localization by adiabatic selective refocusing; PCA, perchloric acid; STE, stimulated echo; tCho, total choline; tCr, total creatine; tNAA, total n-acetylaspartate; VAPOR, VAriable Power radiofrequency pulses with Optimized Relaxation delays.

This is an open access article under the terms of the Creative Commons Attribution-NonCommercial License, which permits use, distribution and reproduction in any medium, provided the original work is properly cited and is not used for commercial purposes.
© 2021 The Authors. *NMR in Biomedicine* published by John Wiley & Sons Ltd.

regions. These original experimental insights should be useful to better interpret and model the diffusion signal of molecules that are distributed between ICS and ECS compartments.

KEYWORDS
apparent diffusion coefficient, brain, diffusion, double diffusion encoding, extracellular space, tortuosity

1 | INTRODUCTION

Brain extracellular space (ECS) acts as an intercellular communication channel deployed as a 3D functional web throughout the brain, displaying gap widths ranging from tens up to several hundreds of nm,[1,2] and occupying about 20% of the total tissue volume.[3–6] The brain ECS is composed of the interstitial fluid filled by large macromolecules—collagen, proteoglycans, hyaluronan and enzymes—that constitute the extracellular matrix (ECM), an essential structural and metabolic support network.[7] Notably, the interstitial fluid comes in close communication with the cerebrospinal fluid (CSF) at the ventricular (choroid plexus), perivascular (blood–brain barrier) and subarachnoid spaces, bringing nutrients, maintaining homeostasis and clearing metabolic waste.[8–11] Furthermore, the brain ECS plays a paramount role in neuronal activity by constituting an ion reservoir that maintains resting and action potentials. The term of "volume transmission" was coined to describe how ECS can be seen as a porous, resistive medium through which signaling molecules can travel, aiding the formation of widespread, complex cellular networks by modulating extrasynaptic neuronal activation.[4,12,13] ECS is therefore an essential compartment of brain tissue. However, it still constitutes some kind of uncharted territory, in particular regarding how molecular diffusion is impacted by ECS microstructure.

This lack of knowledge severely limits our ability to interpret molecular diffusion, as measured by diffusion-weighted MRI (DW-MRI), in terms of microstructure. DW-MRI allows measuring diffusion properties of water molecules over a distance of 1–20 μm using diffusion-sensitizing gradients.[14,15] Nevertheless, this approach only provides a picture of diffusion properties averaged at a macroscopic resolution (the resolution of the MRI image). Considerable efforts have been deployed by the community to infer quantitative microstructural parameters (such as fibers orientation and density, axon diameter) using models describing diffusion in some parameterized microstructure.[16,17] However, due to the ubiquitous nature of water molecules, these approaches have to rely on strong priors about the diffusion properties of water molecules in the different compartments composing the tissue, in particular ECS versus ICS. Some of these priors remain to be experimentally validated, in particular: Is diffusion faster in ECS compared with ICS? Can diffusion in ECS be considered Gaussian, that is, following similar laws as free diffusion? In DW-MRI, many studies have attempted to tackle this problem in white matter by proposing a variety of additional contrasts combined with diffusion tensor or diffusion kurtosis imaging (DTI/DKI). This strategy allows modulating the relative contributions of the intracellular and extracellular compartments to the total diffusion signal and analyzing how this affects the diffusion metrics subsequently derived from biophysical modeling. These original approaches included gadolinium infusion,[18] double diffusion encoding (DDE),[19] planar filtering[20] and measurements at different diffusion times.[21] These studies suggested that parallel intra-axonal water diffusion was either higher[18,20,21] than or similar[19] to parallel extra-axonal water diffusion. However, while these results offer valuable prior knowledge enabling more accurate modeling of DW-MRI data, they only apply to water diffusion in white matter and bring only partial information regarding the diffusion properties in ECS (e.g., they tell us nothing about the Gaussianity).

By contrast, diffusion-weighted nuclear magnetic resonance spectroscopy (DW-MRS) offers a more specific exploration of diffusion than DW-MRI, by allowing direct characterization of the diffusion properties of brain metabolites confined within ICS. A notable exception is that of glucose and lactate, which are present in both ECS and ICS. Interestingly, it was shown by Pfeuffer et al.[22] that glucose and lactate exhibited different diffusion properties from intracellular metabolites, with faster initial signal drop as diffusion-weighting b is increased. More recently, similar behavior was reported for acetate following i.v. acetate infusion.[23] This suggested that signal contribution from ECS quickly disappeared due to fast diffusion, which, with the additional (and implicit) assumption of mono-exponential signal attenuation in ECS, allowed the authors to estimate the extracellular fraction of these compounds. Such a noninvasive DW-MRS approach might actually be very useful to study lactate compartmentation, as lactate release in ECS (in the framework of the hypothetical astrocyte-to-neuron lactate shuttle) might be crucial for brain function.[24,25] However, like for DW-MRI modeling, prior knowledge regarding diffusion in ECS is required to disentangle its contribution to the overall diffusion signal.

Unfortunately, no NMR-detectable endogenous metabolite or ion solely resides in the brain ECS. Consequently, to experimentally characterize diffusion properties in ECS, one has to rely on the use of an injected exogenous marker. Such a marker should be strictly confined within ECS, be of relatively similar size to water or endogenous metabolites to allow for relevant comparison, and neither perturb the osmotic equilibrium nor induce deleterious metabolic reactions. Tracking the diffusion of such probes can therefore help with retrieving precious information on ECS microstructural conformation in both normal and pathological states, and has indeed been quite extensively performed using non-MR

probes.[6,26,27] Several approaches using radiotracers,[28–30] real-time iontophoresis[26,31–36] and advanced optical imaging techniques[1,2,37–43] have been proposed to accurately quantify the apparent diffusion coefficient (ADC) and tortuosity λ, where (D_{free} being the free diffusion coefficient of the molecule of interest):

$$\lambda = \sqrt{\frac{D_{free}}{ADC}}. \quad (1)$$

Most commonly reported ECS λ values are approximately 1.6, reflecting diffusion greatly hindered by a variety of microstructural features such as cells, a high number of deadspace microdomains and, for some probes, electrostatic interactions with the numerous negative charges present in the ECM and binding to active sites located on cell membranes or the ECM.[44–49]

In the field of MR in vivo, a series of pioneering experiments in DW-MRS have been proposed by the team of Neil and Ackerman to estimate ADC and λ metrics in ECS.[50–54] They used a broad range of spectroscopic modalities (^{1}H, ^{23}Na, ^{19}F) and ECS markers to compare intracellular and extracellular diffusion properties in the rodent brain, under both healthy and ischemic conditions. Despite the great insights into the nature of diffusion in ECS provided by these studies, they led to somewhat inconclusive data: while ADC values inferred from ^{19}F or ^{1}H DW-MRS experiments did not support any clear difference between ECS and ICS, data obtained with ^{23}Na DW-MRS indicated otherwise, that is, more than two-fold faster diffusion in ECS compared with ICS. The lack of specificity to ECS of some exogenous markers was proposed as the main explanation for these contradictory results.[52] Additionally, these studies were performed at fixed diffusion time (t_d) and relatively low diffusion weighting (b), thus allowing only quantification of ADC and tortuosity, which does not reflect the broad range of diffusion properties that can be measured (and potentially modeled) with modern DW-MRI and DW-MRS experiments.

The aim of the present work is to revisit MR-measured extracellular diffusion properties and, in particular, to go beyond the sole quantification of the ADC and tortuosity metrics by proposing a thorough assessment of extracellular diffusion properties. To this end, we use state-of-the-art DW-MRS acquisition and processing strategies, while benefiting from the exquisite sensitivity of a ^{1}H cryoprobe at 11.7 T. First, a solution of sucrose, a well-known marker of ECS due to the absence of sucrose transporter in the mammal brain,[28] is slowly infused in the mouse brain, either inside ventricles close to the hippocampus or in the prefrontal cortex. We then perform, in a voxel localized close to the injection site, that is, either around the hippocampus or in the prefrontal cortex, three types of DW-MRS acquisitions in vivo to obtain complementary information on several key microstructural features[55–58]: (1) short-range restriction using measurements at high b-values up to 30 ms/μm^2; (2) longer-range structures via ADC measurements for t_d increasing up to 1 s; and (3) microscopic anisotropy, as revealed by DDE. We finally confirm, using cell dissociation followed by HR-MAS spectroscopy, that sucrose indeed remains in ECS.

2 | METHODS

2.1 | Animal experiments

All experimental protocols were reviewed and approved by the local ethics committee (CETEA no. 44), and authorized by the French Ministry of Education and Research. They were performed in an approved facility (authorization #B92–032-02), in strict accordance with recommendations of the European Union (2010–63/EEC). All efforts were made to minimize animal suffering, and animal care was supervised by veterinarians and animal technicians. Mice were housed under standard environmental conditions (12-h light–dark cycle, temperature: 22 ± 1°C and humidity: 50%) with ad libitum access to food and water.

2.2 | Stereotaxic surgery

Infusion of a 1 M sucrose solution was performed using stereotaxic surgery. Briefly, C57BL/6 J wild-type mice were anesthetized with 1.5% isoflurane in an O_2/air mixture and positioned in a stereotaxic frame. Stereotaxic cannula (ø = 160 μm) were inserted following local anesthesia using subcutaneous administration of a 5 mg/mL lidocaine solution, skin incision and skull perforation. Two injection sites were investigated in the context of this study: (1) injection in lateral ventricles (anteroposterior/ mediolateral/ dorsoventral relative to bregma [AP/ML/DV]= ±1/-0.2/-2.1 mm, the latter being from the dura mater) at a rate of 0.5 μL/min for 30 min and (2) injection in prefrontal cortex tissue ([AP/ML/DV]= ±1.5/+2/−1.2 mm, the latter being from the dura mater) at a rate of 0.1 μL/min for 30 min. After the whole volume of sucrose solution was injected, the cannula was left in place for 10 min before removal to prevent capillary suction of sucrose out of the tissues. The mouse was then transferred to the MRI room after stitching the skin of the animal (the dura was not repaired).

2.3 | DW-MRS in vivo

MRI scans were performed in an 11.7 T scanner (Bruker, Ettlingen, Germany) with maximal gradient strength on each axis G_{max} = 752 mT/m, using a quadrature surface cryoprobe. Mice anesthesia was maintained with 1.5% isoflurane in O_2/air mixture. Considering the time required for transferring the animal, placing it in a dedicated scanning bed and performing the necessary preliminary adjustments (frequency tuning, impedance matching, shimming), acquisition started 45 to 60 min following the end of sucrose injection.

Four mice were used for each acquisition protocol and each injection site. When the stereotaxic infusion was performed in the lateral ventricles, an acquisition voxel of $7 \times 3 \times 3$ mm^3 was positioned around the hippocampus, so that the volume occupied by ventricles within the voxel was minimized as much as possible (corresponding in the end to 3%–5% of the total voxel volume). Some limited control experiments were performed in a $2 \times 2 \times 2$ mm^3 voxel containing no ventricles at all, to check that CSF contamination from ventricles did not dominate the measurement in the case of the large voxel. When injection was performed in the prefrontal cortex, a $4 \times 2 \times 2$ mm^3 acquisition voxel containing almost no CSF from ventricles was positioned between the injection sites in the prefrontal cortex. However, we could not completely exclude injection sites from the prefrontal cortex voxel, hence a smaller $2 \times 2 \times 2$ mm^3 voxel excluding injection sites was also used for some control experiments.

A total of 128 repetitions was acquired for each b-value, t_d and DDE ψ angle (more precisely, for each acquisition protocol, the total number of repetitions was split into four blocks of 32 repetitions interleaved with other b, t_d or ψ values). All acquisitions were performed in random order to exclude any possible bias arising from shim degradation or nonsteady-state sucrose concentration/distribution over time. In the case of control experiments in the $2 \times 2 \times 2$ mm^3 voxel, signal was accumulated over a total of 512 repetitions split into 16 blocks of 32 repetitions for b = 0.02 ms/μm^2 and b = 20 ms/μm^2.

Water signal was suppressed using a VAPOR module.[59] Signal processing was performed as described in Ligneul et al.[55] More precisely, scan-to-scan phase and frequency correction were performed using homemade Matlab routines before LCModel analysis.[60] When needed, singular value decomposition[61,62] was performed for additional suppression of water contamination at long t_d. Sucrose spectra acquired in a 50 mM phantom solution with the same experimental t_d values as in our in vivo measurements were added to LCModel's basis set. Similarly, macromolecule spectra were acquired on C57BL/6 J wild-type mice using the same experimental parameters and included in LCModel's basis set. LCModel uses all peaks simultaneously to perform a linear combination of all metabolite spectra comprised in the basis set, thus allowing more accurate fitting than when taking into account single resonances only. Details of the different diffusion measurements are given below.

2.3.1 | High b-values and ADC measurements at long t_d

Measurements were performed using the STE-LASER sequence,[55] which consists of a stimulated echo (STE) diffusion module followed by a LASER localization scheme (TE_STE/TE_LASER = 8/25 ms). For the LASER localization, 2 ms hyperbolic secant pulses (10 kHz bandwidth centered at 3 ppm, i.e., on total creatine signal) were used. In the STE diffusion module, diffusion gradient duration (δ) was equal to 3 ms, and diffusion gradients were applied simultaneously along all three axes with the same strength. In the case of high b-value measurements, the mixing time (TM) was set to 50 ms, corresponding to a t_d of 53.2 ms while diffusion weighting was gradually increased up to 20 ms/μm^2 in the hippocampal voxel and up to 30 ms/μm^2 in the prefrontal cortex voxel. Signal attenuation reported for high b-value measurements corresponds to $ln\left(\frac{S_b}{S_{b=0.02\ ms/\mu m^2}}\right)$, with b = 0.02, 3.02, 5, 10, 20 and 30 ms/μm^2. ADC values were acquired at t_d = 53.2, 253.2, 503.2 and 1003.2 ms by varying TM and acquiring the diffusion signal at b = 0.02 ms/μm^2 and b = 3.02 ms/μm^2 for each TM, with $ADC = \frac{-1}{\Delta b} \times ln\left(\frac{S_{b=3.02\ ms/\mu m^2}}{S_{b=0.02\ ms/\mu m^2}}\right)$.

2.3.2 | Double diffusion encoding

DDE was performed using the sequence described in Vincent et al.[58] Briefly, the sequence comprises two 180° pulses, each flanked by a pair of diffusion gradients, followed by a LASER localization module, as described above (TE_SE/TE_LASER = 71.2/25 ms). The t_d was 28.5 ms for each block while the TM between the two diffusion blocks was fixed at 5.5 ms and δ was equal to 4.5 ms. A total diffusion weighting of 5 ms/μm^2 was applied, that is, 2.5 ms/μm^2 for each diffusion block. The first pair of diffusion gradients was applied along the X direction while the direction of the second diffusion gradient pair was varied in the XY plane, so that the angle ψ described by the two blocks was varied from ψ = 0 to 360° by 45° increments. Signal attenuation reported here corresponds to the ratio $\frac{S_{\psi,\ b=5\ ms/\mu m^2}}{S_{\psi=0,\ b=0.04\ ms/\mu m^2}}$.

2.4 | Measurement of the sucrose free diffusion coefficient

A 50 mM sucrose solution was used to estimate the sucrose D_{free} value at 37°C. To do so, an Eppendorf tube was filled with the solution. A water-circulating heating system was wrapped around the Eppendorf tube, while a temperature-monitoring probe was carefully positioned onto

the tube so that it did not come into direct contact with the heating system. The diffusion signal was acquired three times for b = 0.01 and b = 1.01 ms/μm^2. The D_{free} value was calculated according to the formula $\frac{-1}{\Delta b} \times ln\left(\frac{S_{b=3.02\ ms/\mu m^2}}{S_{b=0.02\ ms/\mu m^2}}\right)$ for each acquisition and the average value over the three measurements was taken as D_{free}, yielding a value of 0.66 ± 0.05 μm^2/ms.

2.5 | Cell dissociation protocol

Four additional mice (two per injection site) were sacrificed 45 min postinjection using neck dislocation. A 1-mm brain slice excluding injection site but containing some part of the corresponding DW-MRS voxel was collected 45 min postinjection and rinsed in Hank's balanced solution (HBSS) solution (sample "ECS 1"). The sample then underwent papain enzymatic digestion (Miltenyi Biotec ref. #130–092-628) followed by mechanical dissociation using homemade glass pipettes of decreasing diameters. The cell suspension was diluted in HBSS solution up to 7 mL and filtered through a 50-μm sieve. The samples were then centrifuged at 300 g for 10 min at room temperature. The remaining top part of about 6 mL was collected (sample "ECS 2") and the cells were gently resuspended in a 500-μL solution of 0.11 M perchloric acid (PCA) solution, thus inducing membrane lysis. The samples were centrifuged at 14,000 g for 15 min at 4°C. Membrane debris precipitated while the intracellular content was collected in the upper phase. The latter was neutralized using a 5 M KOH solution and underwent a second centrifugation round, yielding approximately 400 μL of intracellular content. In order to compensate for the volume difference between the samples and allow for subsequent HR-MAS measurement, all fractions were freeze-dried and pooled together when necessary before being resuspended in D_2O water.

2.6 | HR-MAS NMR spectroscopy

The lyophilized samples were dissolved in D_2O (with 0.05 wt % TSP, Sigma) and pipetted into a 30-μL Kel-F rotor insert for NMR acquisitions. ^{1}H HR-MAS NMR experiments were carried out on a Bruker Avance II, operating at an ^{1}H frequency of 499.16 MHz with HR-MAS under a sample spinning at 4000 Hz at a temperature of 23 ± 2°C. The spectra were acquired by Carr-Purcell-Meiboom-Gill pulse experiment with a TE of 80 ms (with an accumulation of 200 intra-echoes), 1 s water-presaturated pulse as a recycle delay, and 20 ppm spectral width with 32 K complex data points. The ^{1}H chemical shift was referenced to the alanine doublet at 1.48 ppm.

3 | RESULTS

3.1 | Injection in ventricles: efficient sucrose delivery and limited CSF contamination in the DW-MRS voxel

Needle tracks due to stereotaxic surgery (indicated by a red arrow) are clearly visible in the sagittal MRI image presented in the top left corner of Figure 1A. Sucrose was efficiently injected in the lateral ventricles, as can be appreciated by looking at the strong sucrose resonances at 3.65, 3.78 and 5.37 ppm on the corresponding ^{1}H DW-MRS spectrum. Interestingly, sucrose peaks vanished when applying a diffusion weighting of 20 ms/μm^2 while the signal of endogenous intracellular metabolites remained clearly measurable, already demonstrating faster sucrose diffusion, without further quantitative analysis.

We verified that (1) sucrose was able to diffuse deep within the tissue and (2) ventricle contamination did not bias our measurements by acquiring DW-MRS spectra in a smaller 2 × 2 × 2 mm^3 voxel that was both far away from the injection sites (the closer voxel's edge being approximately 1 mm away from the injection site) and did not contain any CSF from ventricles. Interestingly, the measured spectra (presented in Figure 1B) displayed a similar diffusion pattern as in Figure 1A, suggesting limited contamination from ventricles and efficient spreading of sucrose within ECS. Sucrose signal also vanished at b = 20 ms/μm^2, demonstrating that the fast diffusion as qualitatively evidenced in the large voxel is not due to diffusion within CSF. However, because signal-to-noise ratio (SNR) was much lower in that small voxel, we could not perform exhaustive characterization of diffusion properties, as described in the next section for the large voxel.

3.2 | Injection in the ventricles: diffusion properties of sucrose in the hippocampus

Sucrose could be reliably quantified in all experiments, with Cramér-Rao Lower Bound (CRLB) values ranging from 1% to 3% for the least favorable acquisition conditions, that is, a high b-value of 20 ms/μm^2 or long t_d of 1003.2 ms, except for two experiments at b = 20 ms/μm^2, where CRLBs were slightly higher (7%/8%).

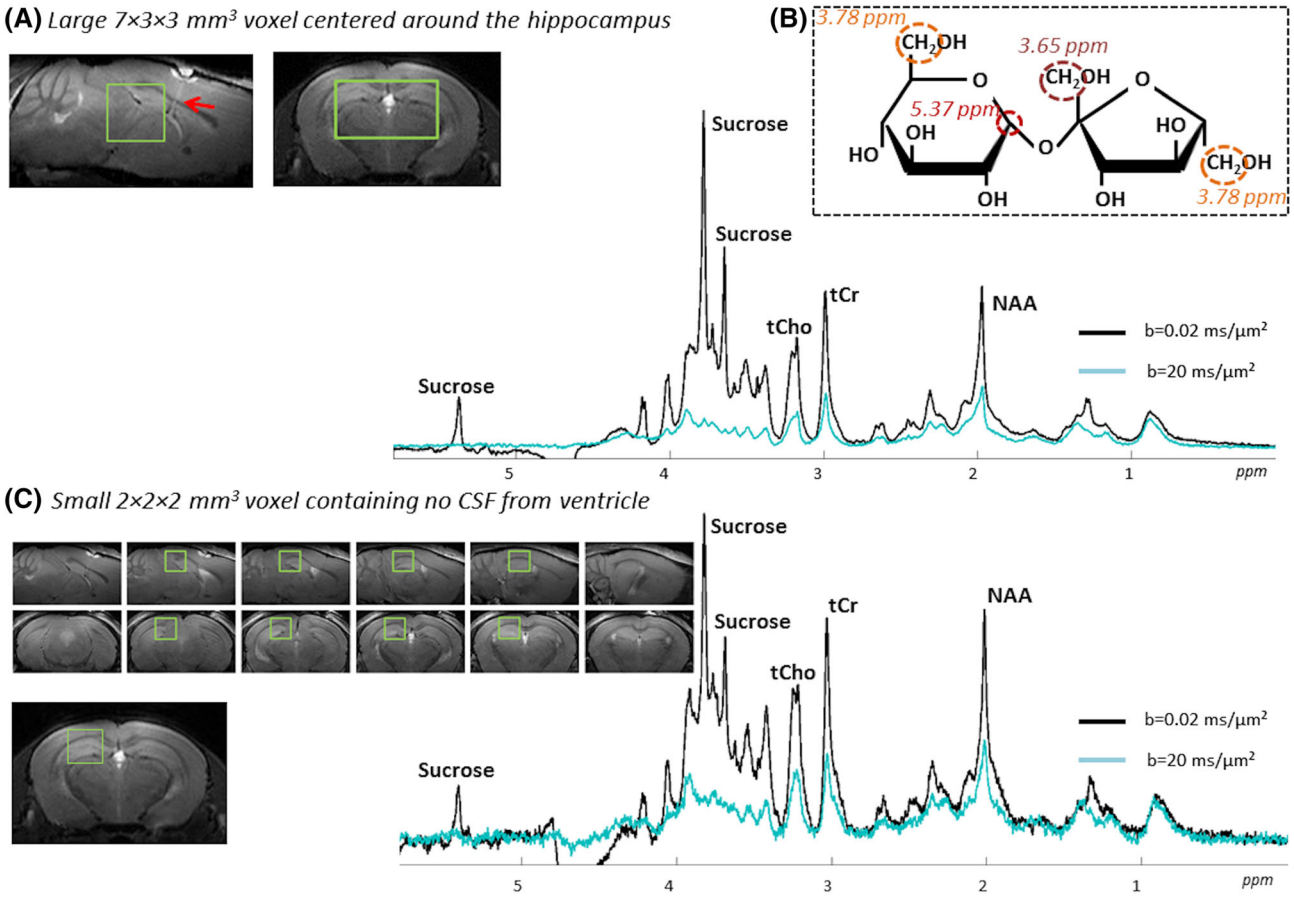


FIGURE 1 A, DW-MRS spectra at b = 0.02 ms/µm^2 and b = 20 ms/µm^2 acquired in a large 7 × 3 × 3 mm^3 voxel positioned in the hippocampus, as shown in the top left corner (the red arrow indicates the needle track). Very strikingly, sucrose resonances vanish at b = 20 ms/µm^2 while intracellular metabolites are still detectable, indicating faster sucrose diffusion. B, Molecular structure of sucrose. The hydrogen atoms corresponding to the three main resonances occurring at 3.65, 3.78 and 5.37 ppm are delineated by circles. C, DW-MRS spectra at b = 0.02 ms/µm^2 and b = 20 ms/µm^2 acquired in a small 2 × 2 × 2 mm^3 voxel containing no CSF or injection sites, as shown on the left side. Strong sucrose signal attenuation, as in the larger voxel, can be observed, suggesting that fast sucrose diffusion is not due to potential bias arising from sucrose diffusing in the CSF. A line-broadening factor of 1 Hz was applied to the data for illustration purposes

Examples of datasets obtained in one animal are shown for the three modalities in Figure 2. Figure 2A shows a dataset acquired for all b-values. A series of spectra acquired in one animal at b = 0.02 and b = 3.02 ms/µm^2 for increasing t_d are presented in Figure 2B. Lastly, an example of a DDE dataset is shown in Figure 2C.

Figure 3A displays the logarithm of signal attenuation averaged over four animals. For purely intracellular metabolites, results are displayed as the mean ± s.d. performed over total n-acetylaspartate (tNAA), total choline (tCho) and total creatine (tCr) data, in order to represent some kind of "intracellular diffusion territory". Spectral contamination due to sucrose signal did not allow highly reliable quantification of weaker overlapping resonances. For this reason, metabolites such as myo-inositol and glutamate were not considered. While sucrose signal attenuation was much stronger than for intracellular metabolites, which confirms faster diffusion as assessed before, it also deviated from mono-exponential behavior at higher b-values (>5 ms/µm^2), indicating some restriction imposed by the local microstructure. Strikingly, lactate signal attenuation exhibits an intermediate pattern, with a strong signal decrease similar to that of sucrose for b-values below 3.02 ms/µm^2 followed by a sharper deviation from mono-exponential attenuation that resembles that of intracellular metabolites. This is in line with the fact that lactate is distributed between ICS and ECS compartments.

ADC values averaged over four animals as a function of t_d are shown in Figure 3B. It can be clearly appreciated that sucrose ADC values are remarkably higher than for intracellular metabolites at all t_d, ranging from 0.24 µm^2/ms at relatively short t_d (53.2 ms) down to 0.22 µm^2/ms at t_d = 1003.2 ms. By comparison, ADC values averaged over the three main intracellular metabolites ranged from 0.095 ± 0.007 µm^2/ms down to 0.079 ± 0.014 µm^2/ms. Interestingly, while ADC values for intracellular metabolites describe a plateau from t_d of 500 ms or higher (which we ascribe to diffusion in long fibers such as axons, dendrites or astrocytic processes[56,57]), sucrose ADC keeps decreasing with t_d, suggesting that the tortuosity regime is not yet reached in ECS. For reference we measured sucrose ADC in a phantom maintained at 37°C, which was found to be

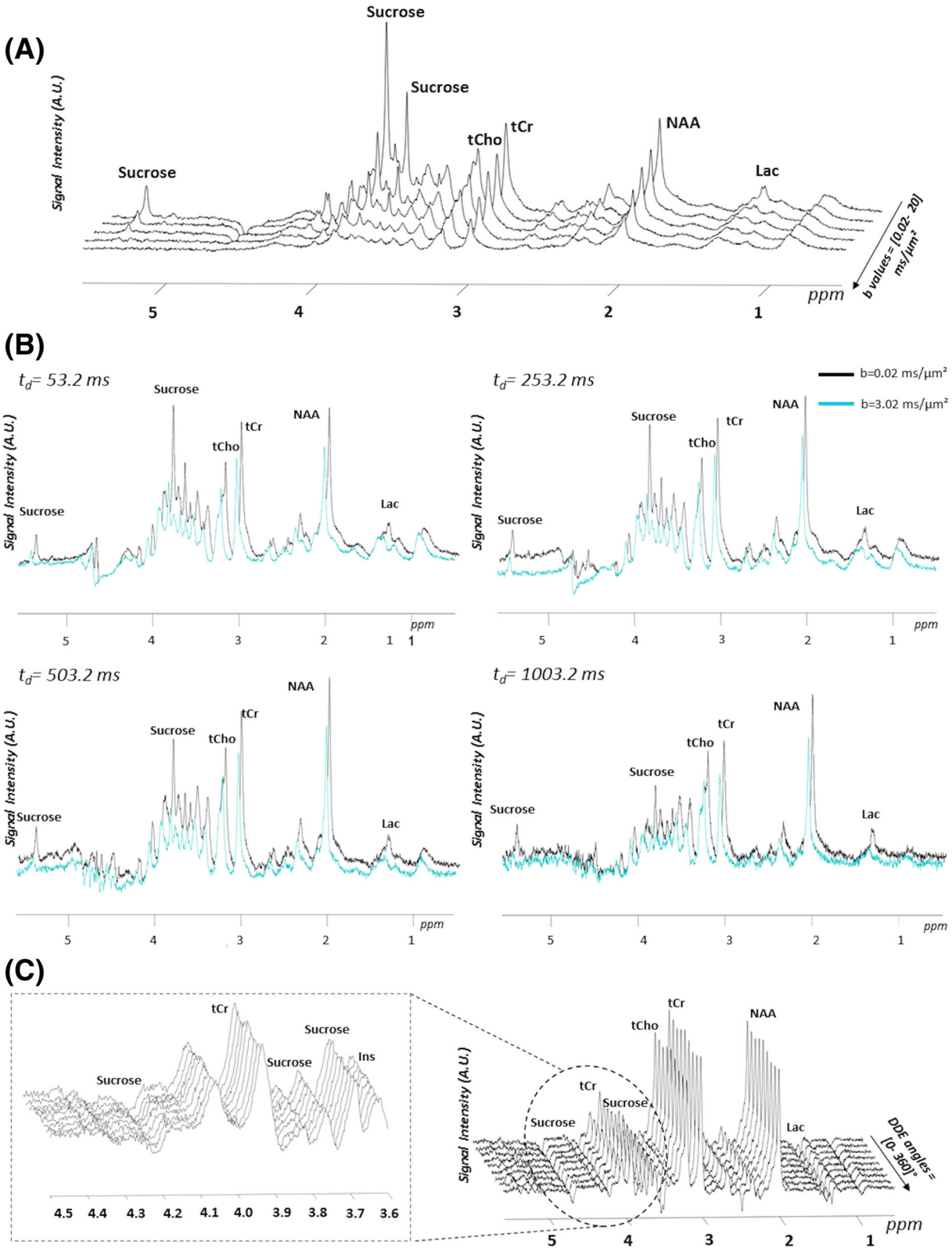


FIGURE 2 A) Example of a dataset acquired for a series of b-values ranging from 0.02 to 20 ms/µm^2 in a 7 × 3 × 3 mm^3 voxel positioned around the hippocampus. Despite exhibiting larger intensity at b = 0.02 ms/µm^2, one can clearly appreciate the stronger signal attenuation for the sucrose resonance compared with that of the three main intracellular metabolites (NAA, tCr, tCho) when increasing b. B, Series of datasets acquired in one animal at two b-values (b = 0.02 ms/µm^2 in black and b = 3.02 ms/µm^2 in blue) for increasing t_d = [53.2; 253.2; 503.2; 1003.2] ms. C, Example of a DDE dataset acquired in one animal (b = 5 ms/µm^2). Signal intensity modulation according to the ψ angle described by the two diffusion gradients is clearly visible for NAA, tCr and tCho. A few resonances such as lactate at 1.3 ppm and MM at 0.9 ppm appear in antiphase due to J-modulation effect. The insert on the left-hand side shows a zoom-in between 3.6 and 4.35 ppm, encompassing the three main sucrose resonances. Signal modulation can be appreciated for tCr while sucrose does not seem to display such behavior (as best visible on the 3.78 ppm resonance). A line-broadening factor of 1 Hz was applied to the data for illustration purposes

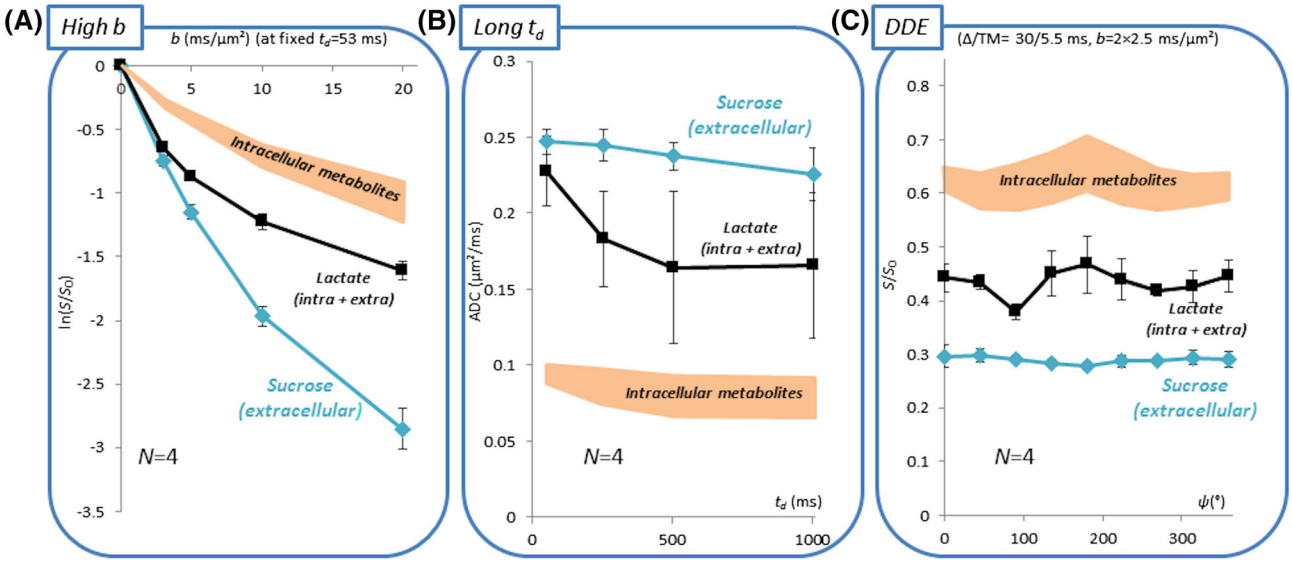


FIGURE 3 A, Logarithm of signal attenuation as a function of b up to 20 ms/μm^2 for intracellular metabolites (average of tNAA, tCho and tCr ± s.d.), lactate (mean ± s.d.) and sucrose (mean ± s.d.). Signal attenuation is markedly stronger for sucrose compared with other metabolites, even though it also deviates from mono-exponential behavior at high b-values, unveiling some short-range restriction. B, ADC time dependency of intracellular metabolites, lactate and sucrose for t_d values ranging from 52.3 up to 1002.3 ms. Sucrose ADC is higher than intracellular metabolite ADC at all t_d. Unlike purely intracellular metabolites, sucrose ADC does not reach a plateau value, suggesting that the tortuosity regime has yet to be reached. C, Signal attenuation as a function of ψ, the angle described by the two pairs of diffusion gradients in the XY plane, in DDE-MRS measurements for intracellular metabolites, lactate and sucrose. While intracellular metabolites display some significant signal angular modulation, sucrose DDE signature remains flat, supporting the idea that it is not diffusing in elongated compartments. For all measurements, lactate displays an intermediate behavior, which is consistent with its distribution among ICS and ECS compartments

0.66 ± 0.05 μm^2/ms, yielding tortuosity values ranging from 1.66 for the lowest t_d value up to 1.73 for a t_d of 1 s. Again, lactate describes an intermediate diffusion behavior, its ADC sharply decreasing at first before stabilizing at approximately 0.17 μm^2/ms for t_d of 503.2 ms or higher.

Average signal angular modulation for intracellular metabolites, lactate and sucrose is displayed in Figure 3C. Intracellular metabolites clearly display signal angular modulation characteristic of diffusing molecules trapped in anisotropic, that is, elongated, compartments. As expected, sucrose signal attenuation is stronger than for intracellular metabolites, which is again consistent with faster diffusion. Very strikingly, sucrose does not exhibit signal angular modulation, that is, there is no indication of sucrose diffusing in elongated pores within the resolution of the measurement. Note that lactate signal attenuation is much stronger than for intracellular metabolites, while displaying some signal angular modulation, but these results are less reliable, since lactate detection is very difficult for the given set of experimental parameters (LCModel's CRLB values of 5%–7% for lactate against 1% for the three main intracellular metabolites).

3.3 | Alternative injection site: diffusion properties of sucrose in the prefrontal cortex

To further rule out any potential contribution of ventricles and assess whether the injection protocol could impact sucrose diffusion measurements, we performed additional experiments where we directly injected sucrose into a prefrontal cortical area with no ventricles (Figure 4A). Despite the smaller voxel size, sucrose, tNAA, tCr and tCho (but not lactate) could still be reliably quantified.

Similar to in the hippocampus, sucrose signal vanished at b = 20 ms/μm^2 despite exhibiting stronger signal intensity at b = 0.02 ms/μm^2, as shown in Figure 4A. To exclude any potential bias possibly arising from the unavoidable presence of the injection sites in this alternative spectroscopic voxel, we performed the same acquisitions in a 2 x 2 x 2 mm^3 control voxel completely excluding the needle track. This acquisition reveals comparable diffusion behavior as in the bigger voxel, thus confirming faster sucrose diffusion (Figure 4B).

The diffusion properties of sucrose in this cortical voxel are presented in Figure 5. For all acquisition protocols, similar trends in diffusion behavior could be observed for both sucrose and ICS metabolites between the two acquisition voxels (hippocampus vs. cortex). In addition to faster diffusion properties, sucrose exhibited nonmono-exponential signal attenuation at higher b-values (Figure 5A). Interestingly, sucrose signal attenuation seems to reflect more pronounced restriction in the prefrontal cortex, which will be further scrutinized in the Discussion section.

Moreover, measurements at long t_d confirm markedly higher ADC values for sucrose compared with intracellular metabolites at all t_d, yielding tortuosity values ranging from λ = 1.59 for t_d = 53.2 ms to λ = 1.62 for t_d = 1003.2 ms (Figure 5B). Even although these values appear slightly

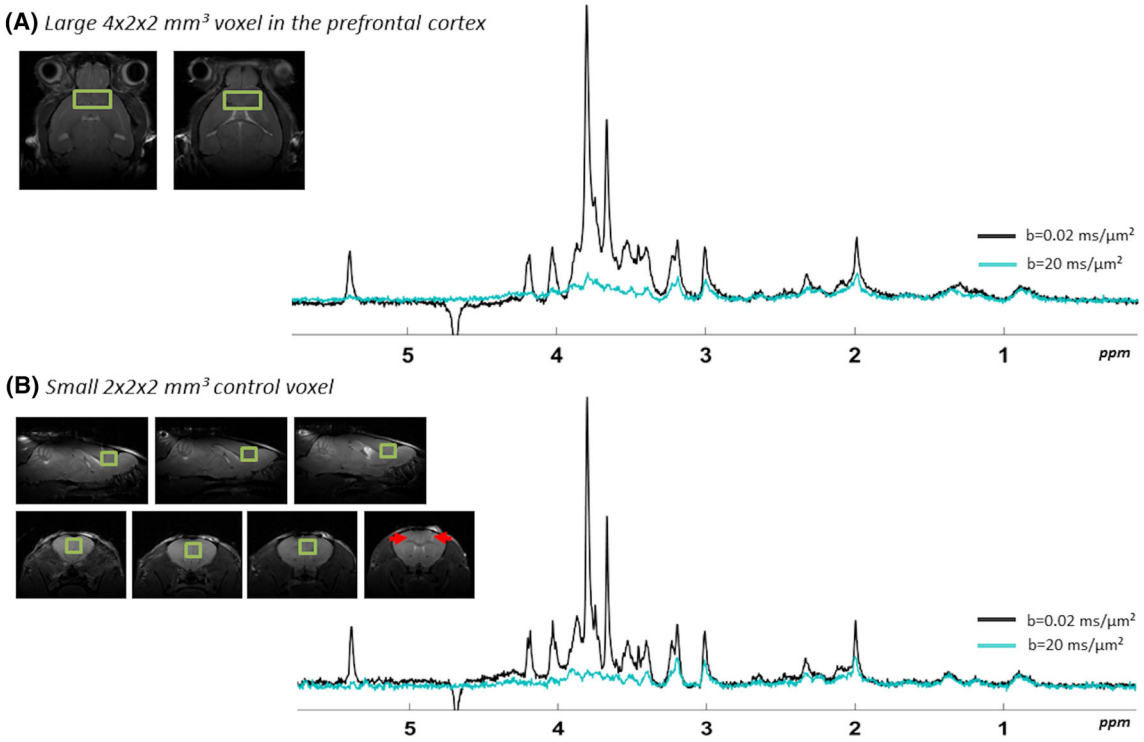


FIGURE 4 A, Axial images of the alternative $4 \times 2 \times 2$ mm^3 voxel positioned in the prefrontal cortex together with two diffusion-weighted acquisitions performed at b = 0.02 ms/µm^2 and b = 20 ms/µm^2. Like in the hippocampus, sucrose signal diffusion appears faster than for intracellular metabolites. B, Left-hand side: sagittal (top line) and coronal (bottom line) anatomical images of a control $2 \times 2 \times 2$ mm^3 voxel positioned in the prefrontal cortex. Needle tracks at injection sites are marked by a red arrow. Right-hand side: spectra acquired at b = 0.02 ms/µm^2 and b = 20 ms/µm^2. Sucrose resonances vanish at higher b-value, revealing similar diffusion behavior as in the bigger experimental voxel

lower than the ones obtained in the hippocampus (where λ = 1.66-1.73), the higher standard deviation associated with our ADC measurements in this smaller voxel precludes concluding in favor of a significant difference in tortuosity between the two brain regions. It also appears that sucrose ADC values do not reach a plateau at longer t_d, suggesting that the tortuosity regime is not fully reached yet in this cortical area.

Lastly, signal angular modulation can also clearly be appreciated for intracellular metabolites while sucrose does not display such behavior, reflecting no detectable microscopic anisotropy, at least not given our current experimental parameters (Figure 5C).

3.4 | Detection of sucrose in extracellular and intracellular fractions following cell dissociation protocol followed by HR-MAS spectroscopy

In order to confirm the absence of sucrose in ICS, we performed a couple of additional experiments where the animals were sacrificed 45 min postinjection to collect brain tissue samples and perform cell dissociation followed by HR-MAS spectroscopy. A schematic description of this protocol, together with the corresponding ICS, membrane and ECS fractions collected at each step of the dissociation process, is available in Figure 6A. Importantly, since all materials collected at the different steps of the dissociation protocol were actually analyzed (nothing was thrown away), all sucrose originally present in the tissue must ultimately be found in the different samples. Hence, a comparison of absolute MR signals was relevant to compare the amount of sucrose in the different samples (Figure 6B). Most of the sucrose was retrieved in the HBSS solution (ECS fraction 1), in which the sample tissue slice was immersed immediately after dissection. Considering $ADC_{sucrose}$ being approximately 0.22 µm^2/ms based on the results presented in the previous section, one can expect sucrose to travel over path lengths of approximately 0.6 mm in 15 min (duration of HBSS rinse). Considering a 1-mm thick tissue slice, it is therefore reasonable that most sucrose initially located deep within the dissected tissue was collected during this step of the protocol. Although it was present in a much lower quantity, some sucrose was also retrieved in the second ECS fraction obtained following enzymatic and mechanical cell dissociation. Most importantly, no sucrose was detected in the ICS fraction or in the membrane debris fraction. This demonstrates the very high ECS specificity of sucrose.

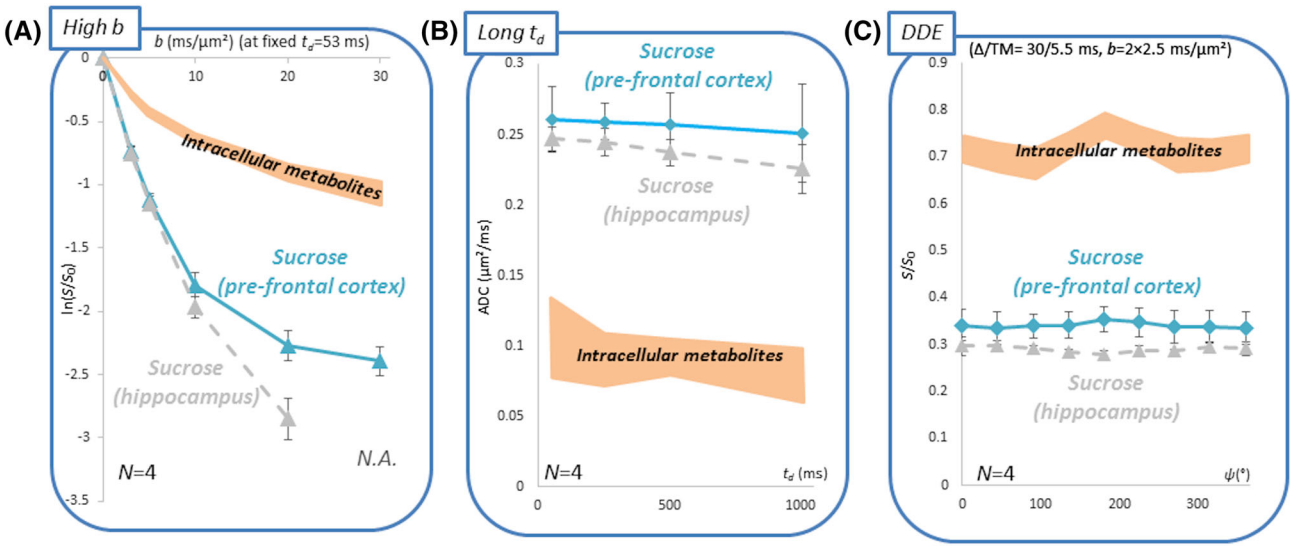


FIGURE 5 A, Logarithm of signal attenuation as a function of b up to 30 ms/µm^2 for intracellular metabolites (average of tNAA, tCho and tCr ± s.d.) in the prefrontal cortex and for sucrose in both prefrontal cortex and, for reminder, in the hippocampus (mean ± s.d. over four animals). Signal attenuation in both voxels display remarkably different behavior, which suggests that sucrose experiences increased short-range restriction in the prefrontal cortex. B, ADC values as a function of time at t_d = 52.3–1002.3 ms, for intracellular metabolites and sucrose in the hippocampus and the prefrontal cortex. A similar behavior as in Figure 3 is observed, and sucrose ADC values between the two areas are not significantly different. C, DDE-MRS experiments for intracellular metabolites and sucrose in the hippocampus and the prefrontal cortex. As in the hippocampal voxel, sucrose DDE-MRS signature remains flat while signal angular modulation can be appreciated for purely intracellular metabolites. Note that lactate could not be reliably quantified in this region, and thus is not reported here

4 | DISCUSSION

4.1 | Potential biases arising from the experimental injection of an exogenous ECS marker

The presence of ventricles in the hippocampus voxel or injection sites in the prefrontal cortex voxel might have potentially biased the results towards faster (and Gaussian) diffusion. However, in the case of the hippocampus, the volume fraction occupied by ventricles in the voxel remains below 5%, and this remains true even considering worst-case chemical shift displacement error (which, in our study, arises for the 5.37 ppm resonance along the dorsoventral direction, for which the actual voxel position is shifted only by 0.36 mm towards the bottom of the brain). Furthermore, additional measurements in small voxels containing no CSF from ventricles or tissues damaged by cannula insertion exhibited an amount of sucrose (relative to intracellular metabolites) and fast sucrose diffusion similar to the large voxel, strongly suggesting that contamination by ventricles or injection sites is not driving diffusion behavior observed in the large voxel.

Another source of bias may be a change in the osmotic balance due to the injection of highly concentrated sucrose solution. Diffusion of intracellular metabolites is however similar to what has been previously observed by our team,[55,56] indicating unaltered cell morphology. Moreover, DTI does not indicate any acute change in water mean diffusivity within the hippocampal voxel following the intraventricular injection protocol (Figure 7A). This, however, is not the case when injecting sucrose directly within the tissues in the prefrontal cortex, as can be seen in Figure 7B. This point will be further examined in the final section of the Discussion.

4.2 | Diffusion in ECS is faster than in ICS…

Our results report that sucrose diffusion in ECS is faster than in ICS. More specifically, sucrose ADC roughly corresponds to one third of its D_{free} value. Comparatively, ADC_{tNAA} is equal to approximately 10% of its D_{free} value (considering a D_{free} of 0.78 µm^2/ms, as measured by Kroenke et al.[63]), which is three times less than for sucrose. These results might appear at first to be in disagreement with the work of Duong et al. reporting little difference between intracellular and extracellular ADC, in a study where ^{19}F-MRS ADC measurements of either extracellular or intracellular 2-[^{19}F]Fluoro-2-deoxyglucose-6-phosphate were performed in rat brain (normal and ischemic).[50] The authors ascribed these rather surprising results to the fact that, even although there is a lower concentration of macromolecules potentially hindering diffusion compared with ICS, molecules trapped in ECS compartment are confined in narrow pathways down to the nanometer scale. Therefore, they may statistically encounter the plasma membrane more often than their intracellular counterparts, where the cell body dimension is by

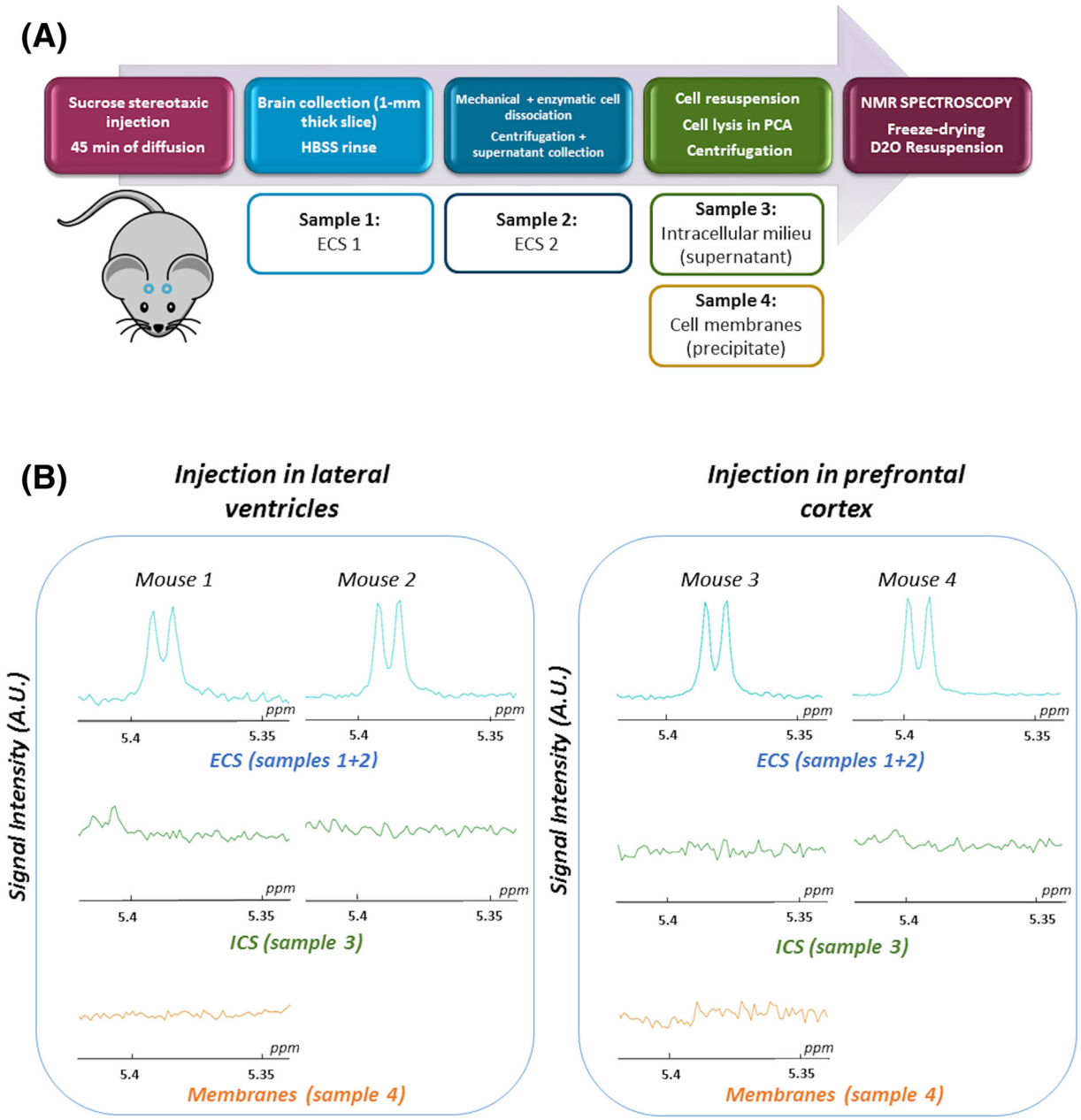


FIGURE 6 A, Summary of the cell dissociation protocol performed prior HR-MAS spectroscopy. Each step of the protocol yields a sample fraction corresponding to ECS, ICS or cell membranes. B, HR-MAS detection of sucrose following the cell dissociation protocol after injection in the lateral ventricles (left-hand side) or directly within the tissues in the prefrontal cortex (right-hand side). Sucrose is mainly retrieved in ECS samples (top spectra) while it can be detected neither in ICS sample (middle spectra) nor on cell membranes (bottom spectra)

comparison an order of magnitude larger, being approximately 10 μm. Later on, Duong et al. performed another series of ^{1}H-MRS experiments by administering, via intraventricular infusion, a variety of exogenous "compartment-selective" ECS markers.[51] As expected, ADC values decreased with molecular weight, ranging from 0.22 down to 0.063 μm^2/ms. The rich information contained in spectra allowed the investigators to directly compare their results with the diffusion of the purely intracellular metabolite NAA. In this study, the ADC of NAA, although unusually high, was not drastically lower than that of ECS markers of comparable hydrodynamic radius such as mannitol (0.16 μm^2/ms for NAA vs. 0.20 μm^2/ms for mannitol).

In our opinion, the discrepancy between their studies and the current study may arise from the fact that sucrose appears to be more specific to ECS than the probes used by Duong et al.[51] For example, based on cell culture experiments, Duong et al. reported a corresponding intracellular fraction of 35% for mannitol. By comparison, our cell dissociation protocol showed no detectable sucrose in ICS or on cell membranes. The experimental timing used in the study of Duong et al., where DW-MRS acquisition started at 4 h postinjection (instead of at approximately 1 h

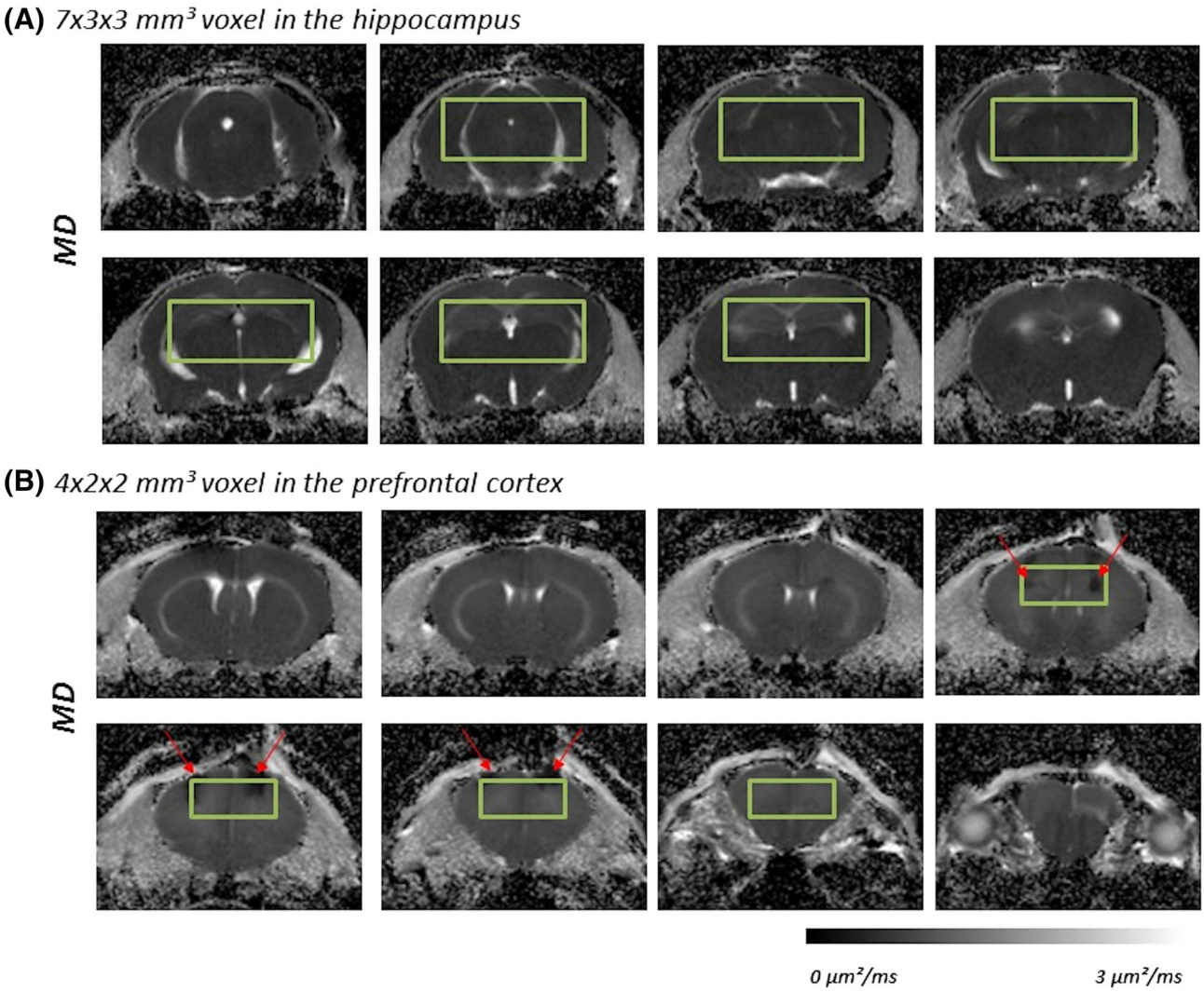


FIGURE 7 A, Mean diffusivity (MD) reconstructed images from DTI acquisition colocalized with the $7 \times 3 \times 3$ mm^3 hippocampal voxel (green rectangle). The MD appears quite uniform throughout the whole voxel, suggesting that the cannula insertion into the ventricles did not induce dramatic damages in the tissue. B, MD maps obtained around the $4 \times 2 \times 2$ mm^3 prefrontal voxel. In this case, while MD again appears quite uniform throughout the voxel, darker spots (indicated by red arrows) are visible around the injection sites, revealing that some small amount of tissue (approximately 6%) contained in the experimental voxel presumably reacted to sucrose injection. Diffusion-weighted images (resolution = 160×160 µm^2, slice thickness = 500 µm) were acquired with an EPI module over 30 directions at b = 1 ms/µm^2, (δ/Δ = 2/20 ms, TE/TR = 30/3200 ms)

postinjection in our case), might also have contributed to a higher fraction of ECS markers penetrating ICS. Such a long incubation time potentially leading to some intercompartment exchange might also partly explain their results with [^{19}F]Fluoro-2-deoxyglucose-6-phosphate.

It is interesting to reanalyze the mannitol data obtained by Duong et al.: considering an overall ADC value of 0.20 µm^2/ms and that 35% of mannitol is in ICS (with $ADC_{ICS} \approx 0.16$ µm^2/ms based on the investigators' data for NAA, which has an almost similar hydrodynamic radius) while 27% of mannitol is subject to nonspecific membrane binding (with $ADC_{membrane} \approx 0.02$ µm^2/ms according to Reed et al.[64]), one can estimate $ADC_{ECS} \sim 0.36$ µm^2/ms in the case of mannitol. In the end, based on mannitol data from Duong et al., one comes up with ADC_{ECS} being more than twice as large as ADC_{ICS}, which is in line with our own ADC measurements.

Consequently, we are overall quite confident in our results, and control experiments in smaller voxels are clearly in favor of faster sucrose diffusion compared with ICS metabolites. Notably, this is consistent with the results reported by Goodman et al.[52] for sodium, which exhibits an 4:1 extracellular-to-intracellular ratio, thus making it a quite specific endogenous marker of ECS. The authors measured the ADC of sodium ion in rat brain using ^{23}Na DW-MRS and reported it to be.1.15 ± 0.09 µm^2/ms, which corresponded to 61% of its D_{free} value measured at 37°C. They performed similar acquisitions for water, estimating that its ADC in brain tissue was 28% of D_{free}. The authors therefore concluded that ADC_{ECS} is approximately two-fold higher than ADC_{ICS}. In a similar spirit, Dehghani et al.[23] compared the diffusion profile of acetate during intravenous infusion with that of purely intracellular NAA. The ADC values for both molecules estimated for b-values inferior to 5 ms/µm^2 yielded

0.24 ± 0.008 μm^2/ms for acetate and 0.086 ± 0.002 μm^2/ms for NAA. This is in surprisingly good agreement with our own results, even although the comparison is limited here by the facts that (1) acetate is a much smaller molecule than sucrose and (2) the extracellular fraction of acetate is estimated to be "only" 40% under the experimental conditions used in this study. Overall, this study also supported the idea of faster diffusion of acetate in ECS.

Lastly, it is interesting to draw a parallel with the studies that were performed in white matter using DW-MRI to disentangle water extra-axonal and intra-axonal parallel diffusivities.[18–21] In first approximation, considering an isotropic orientation distribution of sticks, the ADC we measured for intracellular metabolites should be equal to approximately Dn/3, Dn being the intracellular diffusion coefficient parallel to neurites. In our study, we found that ADC_{NAA} was approximately 10% of its D_{free}, thus corresponding to Dn being approximately 30% of D_{free} for the intra-neuronal marker NAA. This is actually very close to the extracellular ADC value for sucrose, that is, $ADC_{sucrose}$ is approximately 33% of its D_{free}. However, we shall stress here that this comparison is limited by the fact that we performed our measurements in a voxel mostly composed of gray matter, which obviously greatly differs from white matter in terms of microstructure: in particular, unlike in white matter axonal bundles, extracellular diffusion cannot be separated into parallel and perpendicular components. Comparison between intra- and extra-axonal parallel diffusivities is therefore beyond the scope of the study.

4.3 | … although diffusion in ECS is also restricted and tortuous

Measurements at high b-values clearly show that sucrose signal attenuation deviates from mono-exponential behavior, which is a manifestation of restriction. Beyond sole cell membranes, we believe that such a restriction might also reflect deadspace microdomains, as unveiled by a large number of previous studies[1,45–47] that suggest these microstructural dead ends may account for about one third of the overall tortuosity.[6]

Our estimation of ECS tortuosity ($\lambda \sim 1.6$ in cortex and $\lambda \sim 1.7$ in the hippocampus) is rather close to what has been previously reported in other studies using real-time iontophoresis or integrative optical imaging ($\lambda \sim 1.6$).[65] However, as the diffusion scales probed in this study (from ~5 to ~20 μm) are smaller than what is typically observed using alternative techniques, some caution shall be applied.[54] In our case, it appears that the tortuosity regime is not reached yet, and longer t_d might have reflected slightly larger tortuosity. What about comparisons with NMR-derived tortuosity? In Duong et al.,[51] the λ value reported for mannitol is rather surprisingly high ($\lambda = 1.83$ for a diffusion distance of approximately 2.8 μm), especially when considering that mannitol is smaller than sucrose and exhibits a hydrodynamic radius similar to that of NAA. The authors proposed that, considering the scale of displacement distances, probe molecules were less likely to be sensitive to perivascular pulsation compared with alternative techniques that sample displacements occurring over hundreds of microns. As discussed before, we believe that this difference might also be due to the fact that mannitol was not completely specific to ECS, thus partly sampling ICS where the ADC is lower and biasing the estimated tortuosity toward larger values.

It would be very insightful to go beyond the simple statement that sucrose ADC is decreasing when t_d is increasing, and to characterize whether it follows some specific power law, in the spirit of theoretical and experimental works from Novikov et al.[66–68] Unfortunately, data are too sparse and s.d. too large to allow for such an analysis.

4.4 | Absence of microscopic anisotropy in ECS

DDE measurements display unparalleled sensitivity to microscopic anisotropy, that is, to diffusion occurring in highly anisotropic structures such as cylinders or elongated pores.[69–71] In such cases, provided that the TM between the two diffusion blocks is long enough, the theoretical analysis of DDE experiments proposed by Mitra indeed predicts that angular dependence of the signal magnitude can be observed, displaying signal maxima in the case of parallel measurements ($\psi = 0$ and 180°) and minima in the case of perpendicular measurements ($\psi = 90$ and 270°).[72] On the contrary, restricted diffusion in isotropic compartments is not expected to yield such modulation.

DDE-MRS of intracellular metabolites has been successfully employed in vivo, showing some significant angular modulation that suggests metabolites mainly diffuse in elongated compartments such as cell fibers.[58,73,74] DDE acquisition parameters used in the present study, that is, low b-value and short TM, were chosen to allow reliable quantification of sucrose signal, and are quite different from those used in past studies focusing on intracellular metabolites.[58,73,74] While we observe such a pattern for the three main intracellular metabolites, DDE-MRS signature of sucrose does not exhibit any signal angular modulation. This supports the view that ECS is not a highly anisotropic structure at microscopic scale, at least in gray matter. Of course, at sub-μm scales (i.e., at the scale of gap width or deadspace microdomains) there is certainly some pronounced anisotropy in ECS, but at the larger scale of the diffusion distance probed during DDE measurements (a few μm), all correlation is lost between the diffusion directions of the two successive diffusion epochs, resulting in the absence of signal modulation. Interestingly, the intermediate behavior displayed by lactate, that is, more pronounced signal attenuation combined with narrower signal intensity angular modulation, is consistent with the fact that lactate is present in both ECS and ICS. These results are in line with past DDE measurements showing limited lactate signal angular modulation compared with purely intracellular metabolites, which considering the results of the present work is due to the presence of an

important extracellular lactate pool with very limited angular modulation.[22,58,73] To the best of our knowledge, this is the first time that DDE-MRS has been specifically performed in ECS, and we believe that DDE might actually be extremely powerful to successfully distinguish between ECS and ICS compartments.

4.5 | Impact of injection protocol

Quite strikingly, measurements at high b-values reveal more significant short-range restrictions for sucrose diffusing in the prefrontal cortex compared with the hippocampus. One explanation could lie in microstructural differences between the two areas, which might be the result of a higher density of deadspace microdomains and/or more packed cells in the prefrontal cortex. However, this result shall be cautiously interpreted as sucrose injection directly within the cortex indisputably constitutes a more damaging process for the tissues compared with intraventricular injection. Indeed, and as mentioned before, water mean diffusivity maps obtained using DTI measurements in the cortical voxel revealed markedly darker spots around the injection sites (Figure 7B), reflecting a local decrease in water ADC (of about 60%, in a volume corresponding to only ~6% of the spectroscopic voxel). This may reflect some very local tissue damage that may induce increased diffusion restriction in our experimental voxel. Another explanation for the observed discrepancies between the two areas might be that some sucrose molecules are able to enter cells damaged due to direct cannula insertion within the tissues, thus partially sampling the ICS. This would be in line with the sharper deviation from mono-exponential signal attenuation at higher b values (compared with data acquired in the hippocampus), as well as the very slight signal angular modulation that could possibly be discerned for sucrose at $\psi = 180^{\circ}$. This interpretation shall nevertheless be nuanced by the fact that cell damage appears to be very local, that is, is not representative of the whole voxel, at least as assessed from DTI measurements, while data from the cell dissociation protocol did not report higher sucrose quantity in the intracellular fraction.

5 | CONCLUSION

In this study, we assessed the diffusion properties of sucrose in the ECS using state-of-the-art DW-MRS protocols. Our results are in favor of approximately two-fold faster diffusion in ECS compared with ICS. However, our measurements also suggest that diffusion in ECS does not mimic that of a free medium, that is, a microenvironment without any kind of restrictive boundaries or obstacles hindering the diffusion process. More precisely, we found a tortuosity of approximately 1.6 that tends to increase with t_d, indicating that the tortuosity regime has not been reached yet for t_d of up to 1 s. High b-values measurements also unveil some sensitivity to short-range restriction. However, sucrose DDE signal modulation appears to be flat and thus qualitatively different from that of intracellular metabolites. We propose that such specific DDE signature may be used to successfully discriminate ECS from ICS compartments.

ACKNOWLEDGEMENTS

We would like to thank Dr Océane Guillemaud for her help regarding the cell dissociation protocol. This project has received funding from the European Research Council (ERC) under the European Union's Horizon 2020 research and innovation programmes (grant agreement no. 818266). The 11.7 T MRI scanner was funded by a grant from "Investissements d'Avenir - ANR-11-INBS-0011 - NeurATRIS: A Translational Research Infrastructure for Biotherapies in Neurosciences".

DATA AVAILABILITY STATEMENT

The data that support the findings of this study are available from the corresponding author upon reasonable request.

ORCID

Alan Wong https://orcid.org/0000-0002-0917-3165
Julien Valette https://orcid.org/0000-0002-2067-5051

REFERENCES

1. Godin AG, Varela JA, Gao Z, et al. Single-nanotube tracking reveals the nanoscale organization of the extracellular space in the live brain. *Nat Nanotechnol.* 2017;12(3):238-243.
2. Thorne RG, Nicholson C. In vivo diffusion analysis with quantum dots and dextrans predicts the width of brain extracellular space. *PNAS.* 2006;103(14):5567-5572.
3. Nicholson C, Hrabětová S. Brain extracellular space: the final frontier of neuroscience. *Biophys J.* 2017;113(10):2133-2142.
4. Marcoli M, Agnati LF, Benedetti F, et al. On the role of the extracellular space on the holistic behavior of the brain. *Rev Neurosci.* 2015;26(5):489-506.
5. Nicholson C, Syková E. Extracellular space structure revealed by diffusion analysis. *Trends Neurosci.* 1998;21(5):207-215.

6. Hrabetova S, Cognet L, Rusakov DA, Nägerl UV. Unveiling the extracellular space of the brain: from super-resolved microstructure to in vivo function. *J Neurosci*. 2018;38(44):9355-9363.
7. Ruoslahti E. Brain extracellular matrix. *Glycobiology*. 1996;6(5):489-492.
8. Zhang ET, Richards HK, Kida S, Weller RO. Directional and compartmentalised drainage of interstitial fluid and cerebrospinal fluid from the rat brain. *Acta Neuropathol*. 1992;83(3):233-239.
9. Matsumae M, Sato O, Hirayama A, et al. Research into the physiology of cerebrospinal fluid reaches a new horizon: intimate exchange between cerebrospinal fluid and interstitial fluid may contribute to maintenance of homeostasis in the central nervous system. *Neurol Med Chir*. 2016;56(7):416-441.
10. Mestre H, Tithof J, Du T, et al. Flow of cerebrospinal fluid is driven by arterial pulsations and is reduced in hypertension. *Nat Commun*. 2018;9(1):1-9.
11. Sakka L, Coll G, Chazal J. Anatomy and physiology of cerebrospinal fluid. *Eur Ann Otorhinolaryngol Head Neck Dis*. 2011;128(6):309-316.
12. Syková E. Extrasynaptic volume transmission and diffusion parameters of the extracellular space. *Neuroscience*. 2004;129(4):861-876.
13. Bikbaev A, Frischknecht R, Heine M. Brain extracellular matrix retains connectivity in neuronal networks. *Sci Rep*. 2015;5(1):1-12.
14. Stejskal EO, Tanner JE. Spin diffusion measurements: spin echoes in the presence of a time-dependent field gradient. *J Chem Phys*. 1965;42(1):288-292.
15. Cory DG. Measurement of translational displacement probabilities by NMR: An indicator of compartmentation. *Magn Reson Med*. 1990;14(3):435-444.
16. Novikov DS, Kiselev VG, Jespersen SN. On modeling. *Magn Reson Med*. 2018;79(6):3172-3193.
17. Alexander DC, Dyrby TB, Nilsson M, Zhang H. Imaging brain microstructure with diffusion MRI: practicality and applications. *NMR Biomed*. 2019;32(4):e3841.
18. Kunz N, da Silva AR, Jelescu IO. Intra- and extra-axonal axial diffusivities in the white matter: Which one is faster? *Neuroimage*. 2018;181:314-322.
19. Skinner NP, Kurpad SN, Schmit BD, Muftuler LT, Budde MD. Rapid in vivo detection of rat spinal cord injury with double-diffusion-encoded magnetic resonance spectroscopy. *Magn Reson Med*. 2017;77(4):1639-1649.
20. Dhital B, Reisert M, Kellner E, Kiselev VG. Intra-axonal diffusivity in brain white matter. *Neuroimage*. 2019;189:543-550.
21. Jespersen SN, Olesen JL, Hansen B, Shemesh N. Diffusion time dependence of microstructural parameters in fixed spinal cord. *Neuroimage*. 2018;182:329-342.
22. Pfeuffer J, Tkáč I, Gruetter R. Extracellular–intracellular distribution of glucose and lactate in the rat brain assessed noninvasively by diffusion-weighted 1H nuclear magnetic resonance spectroscopy in vivo. *J Cereb Blood Flow Metab*. 2000;20(4):736-746.
23. Dehghani M, Kunz N, Lanz B, Yoshihara HAI, Gruetter R. Diffusion-weighted MRS of acetate in the rat brain. *NMR Biomed*. 2017;30(10):e3768.
24. Pellerin L, Magistretti PJ. Glutamate uptake into astrocytes stimulates aerobic glycolysis: a mechanism coupling neuronal activity to glucose utilization. *PNAS*. 1994;91(22):10625-10629.
25. Suzuki A, Stern SA, Bozdagi O, et al. Astrocyte-neuron lactate transport is required for long-term memory formation. *Cell*. 2011;144(5):810-823.
26. Vorříšek I, Syková E. Ischemia-induced changes in the extracellular space diffusion parameters, K+, and pH in the developing rat cortex and corpus callosum. *J Cereb Blood Flow Metab*. 1997;17(2):191-203.
27. Syková E, Mazel T, Vargová L, Vorříšek I, Prokopová-Kubinová Š. Extracellular space diffusion and pathological states. In: *Progress in Brain Research*. Elsevier; 2000:155-178.
28. Levin V, Fenstermacher J, Patlak C. Sucrose and inulin space measurements of cerebral cortex in four mammalian species. *Am J Physiol-Legacy Content*. 1970;219(5):1528-1533.
29. Fenstermacher JD, Li C-L, Levin VA. Extracellular space of the cerebral cortex of normothermic and hypothermic cats. *Exp Neurol*. 1970;27(1):101-114.
30. Fenstermacher J, Kaye T. Drug "diffusion" within the brain. *Ann N Y Acad Sci*. 1988;531(1):29-39.
31. Nicholson C, Phillips JM. Ion diffusion modified by tortuosity and volume fraction in the extracellular microenvironment of the rat cerebellum. *J Physiol*. 1981;321(1):225-257.
32. Lundbæk JA, Hansen AJ. Brain interstitial volume fraction and tortuosity in anoxia. Evaluation of the ion-selective micro-electrode method. *Acta Physiol Scand*. 1992;146(4):473-484.
33. Lehmenkühler A, Syková E, Svoboda J, Zilles K, Nicholson C. Extracellular space parameters in the rat neocortex and subcortical white matter during postnatal development determined by diffusion analysis. *Neuroscience*. 1993;55(2):339-351.
34. Vorříšek I, Syková E. Evolution of anisotropic diffusion in the developing rat corpus callosum. *J Neurophysiol*. 1997;78(2):912-919.
35. Perez-Pinzon MA, Tao L, Nicholson C. Extracellular potassium, volume fraction, and tortuosity in rat hippocampal CA1, CA3, and cortical slices during ischemia. *J Neurophysiol*. 1995;74(2):565-573.
36. McBain CJ, Traynelis SF, Dingledine R. Regional variation of extracellular space in the hippocampus. *Science*. 1990;249(4969):674-677.
37. Tønnesen J, Inavalli VVGK, Nägerl UV. Super-resolution imaging of the extracellular space in living brain tissue. *Cell*. 2018;172(5):1108-1121.
38. Nicholson C, Tao L. Hindered diffusion of high molecular weight compounds in brain extracellular microenvironment measured with integrative optical imaging. *Biophys J*. 1993;65(6):2277-2290.
39. Zhang H, Verkman AS. Microfiberoptic measurement of extracellular space volume in brain and tumor slices based on fluorescent dye partitioning. *Biophys J*. 2010;99(4):1284-1291.
40. Magzoub M, Zhang H, Dix JA, Verkman AS. Extracellular space volume measured by two-color pulsed dye infusion with microfiberoptic fluorescence photodetection. *Biophys J*. 2009;96(6):2382-2390.
41. Zheng K, Jensen TP, Savtchenko LP, Levitt JA, Suhling K, Rusakov DA. Nanoscale diffusion in the synaptic cleft and beyond measured with time-resolved fluorescence anisotropy imaging. *Sci Rep*. 2017;7(1):1-10.
42. Wolak DJ, Pizzo ME, Thorne RG. Probing the extracellular diffusion of antibodies in brain using in vivo integrative optical imaging and ex vivo fluorescence imaging. *J Control Release*. 2015;197:78-86.
43. Paviolo C, Soria FN, Ferreira JS, et al. Nanoscale exploration of the extracellular space in the live brain by combining single carbon nanotube tracking and super-resolution imaging analysis. *Methods*. 2020;174:91-99.
44. Chen KC, Nicholson C. Changes in brain cell shape create residual extracellular space volume and explain tortuosity behavior during osmotic challenge. *PNAS*. 2000;97(15):8306-8311.

45. Hrabe J, Hrabětová S, Segeth K. A model of effective diffusion and tortuosity in the extracellular space of the brain. *Biophys J.* 2004;87(3):1606-1617.
46. Hrabětová S, Nicholson C. Contribution of dead-space microdomains to tortuosity of brain extracellular space. *Neurochem Int.* 2004;45(4):467-477.
47. Tao A, Tao L, Nicholson C. Cell cavities increase tortuosity in brain extracellular space. *J Theor Biol.* 2005;234(4):525-536.
48. Thorne RG, Lakkaraju A, Rodriguez-Boulan E, Nicholson C. In vivo diffusion of lactoferrin in brain extracellular space is regulated by interactions with heparan sulfate. *PNAS.* 2008;105(24):8416-8421.
49. Hrabětová S, Masri D, Tao L, Xiao F, Nicholson C. Calcium diffusion enhanced after cleavage of negatively charged components of brain extracellular matrix by chondroitinase ABC. *J Physiol.* 2009;587(16):4029-4049.
50. Duong TQ, Ackerman JJH, Ying HS, Neil JJ. Evaluation of extra- and intracellular apparent diffusion in normal and globally ischemic rat brain via 19F NMR. *Magn Reson Med.* 1998;40(1):1-13.
51. Duong TQ, Sehy JV, Yablonskiy DA, Snider BJ, Ackerman JJH, Neil JJ. Extracellular apparent diffusion in rat brain. *Magn Reson Med.* 2001;45(5):801-810.
52. Goodman JA, Kroenke CD, Bretthorst GL, Ackerman JJH, Neil JJ. Sodium ion apparent diffusion coefficient in living rat brain. *Magn Reson Med.* 2005;53(5):1040-1045.
53. Quirk JD, Bretthorst GL, Duong TQ, et al. Equilibrium water exchange between the intra- and extracellular spaces of mammalian brain. *Magn Reson Med.* 2003;50(3):493-499.
54. Kroenke CD, Ackerman JJH, Neil JJ. Magnetic resonance measurement of tetramethylammonium diffusion in rat brain: Comparison of magnetic resonance and ionophoresis in vivo diffusion measurements. *Magn Reson Med.* 2003;50(4):717-726.
55. Ligneul C, Palombo M, Valette J. Metabolite diffusion up to very high b in the mouse brain in vivo: Revisiting the potential correlation between relaxation and diffusion properties. *Magn Reson Med.* 2017;77(4):1390-1398.
56. Palombo M, Ligneul C, Najac C, et al. New paradigm to assess brain cell morphology by diffusion-weighted MR spectroscopy in vivo. *PNAS.* 2016;113(24):6671-6676.
57. Najac C, Branzoli F, Ronen I, Valette J. Brain intracellular metabolites are freely diffusing along cell fibers in grey and white matter, as measured by diffusion-weighted MR spectroscopy in the human brain at 7 T. *Brain Struct Funct.* 2016;221(3):1245-1254.
58. Vincent M, Palombo M, Valette J. Revisiting double diffusion encoding MRS in the mouse brain at 11.7T: Which microstructural features are we sensitive to? *Neuroimage.* 2020;207:116399.
59. Tkáč I, Starčuk Z, Choi I-Y, Gruetter R. In vivo 1H NMR spectroscopy of rat brain at 1 ms echo time. *Magn Reson Med.* 1999;41:649-656.
60. Provencher SW. Estimation of metabolite concentrations from localized in vivo proton NMR spectra. *Magn Reson Med.* 1993;30(6):672-679.
61. van den Boogaart A, van Ormondt D, Pijnappel WWF, de Beer R, Ala-Korpela M, McWhirter JG. Removal of the water resonance from 1H magnetic resonance spectra. In: *Mathematics in signal processing III*. Oxford, UK: Clarendon Press; 1994:175-195.
62. Pijnappel WWF, van den Boogaart A, de Beer R, van Ormondt D. SVD-based quantification of magnetic resonance signals. *J Magn Reson.* 1992;97(1):122-134.
63. Kroenke CD, Ackerman JJH, Yablonskiy DA. On the nature of the NAA diffusion attenuated MR signal in the central nervous system. *Magn Reson Med.* 2004;52(5):1052-1059.
64. Reed RA, Mattai J, Shipley GG. Interaction of cholera toxin with ganglioside GM1 receptors in supported lipid monolayers. *Biochemistry.* 1987;26:824-832.
65. Nicholson C, Kamali-Zare P, Tao L. Brain extracellular space as a diffusion barrier. *Comput Visual Sci.* 2011;14(7):309-325.
66. Novikov DS, Jensen JH, Helpern JA, Fieremans E. Revealing mesoscopic structural universality with diffusion. *PNAS.* 2014;111(14):5088-5093.
67. Fieremans E, Burcaw LM, Lee H-H, Lemberskiy G, Veraart J, Novikov DS. In vivo observation and biophysical interpretation of time-dependent diffusion in human white matter. *Neuroimage.* 2016;129:414-427.
68. Lee H-H, Fieremans E, Novikov DS. What dominates the time dependence of diffusion transverse to axons: Intra- or extra-axonal water? *Neuroimage.* 2018;182:500-510.
69. Shemesh N, Özarslan E, Komlosh ME, Basser PJ, Cohen Y. From single-pulsed field gradient to double-pulsed field gradient MR: gleaning new microstructural information and developing new forms of contrast in MRI. *NMR Biomed.* 2010;23(7):757-780.
70. Özarslan E, Basser PJ. Microscopic anisotropy revealed by NMR double pulsed field gradient experiments with arbitrary timing parameters. *J Chem Phys.* 2008;128(15):154511.
71. Özarslan E. Compartment shape anisotropy (CSA) revealed by double pulsed field gradient MR. *J Magn Reson.* 2009;199(1):56-67.
72. Mitra PP. Multiple wave-vector extensions of the NMR pulsed-field-gradient spin-echo diffusion measurement. *Physical Review B.* 1995;51(21):15074-15078.
73. Shemesh N, Rosenberg JT, Dumez J-N, Muniz JA, Grant SC, Frydman L. Metabolic properties in stroked rats revealed by relaxation-enhanced magnetic resonance spectroscopy at ultrahigh fields. *Nat Commun.* 2014;5:4958.
74. Shemesh N, Rosenberg JT, Dumez J-N, Grant SC, Frydman L. Distinguishing neuronal from astrocytic subcellular microstructures using in vivo Double Diffusion Encoded 1H MRS at 21.1 T. *PLoS One.* 2017;12(10):e0185232.

How to cite this article: Vincent M, Gaudin M, Lucas-Torres C, Wong A, Escartin C, Valette J. Characterizing extracellular diffusion properties using diffusion-weighted MRS of sucrose injected in mouse brain. *NMR in Biomedicine.* 2021;e4478. https://doi.org/10.1002/nbm.4478